The Santa Cruz Eddy. Part I: Observations and Statistics

CRISTINA L. ARCHER, MARK Z. JACOBSON, AND FRANCIS L. LUDWIG

Stanford University, Stanford, California

(Manuscript received 25 March 2004, in final form 30 August 2004)

ABSTRACT

A shallow cyclonic circulation that occurs in the summertime over the Monterey Bay (California) is investigated. Since it is often centered offshore from the city of Santa Cruz and has never been studied in detail before, it is named the Santa Cruz eddy (SCE) in this study. Its horizontal size is 10–40 km, and its vertical extent is 100–500 m. The SCE is important for local weather because it causes surface winds along the Santa Cruz coast to blow from the east instead of from the northwest, the latter being the climatological summer pattern for this area. As a consequence of the eddy, cool and moist air is advected from the south and southeast into the Santa Cruz area, bringing both relief from the heat and fog to the city.

The SCE is unique in its high frequency of occurrence. Most vortices along the western American coast form only during unusual weather events, whereas the SCE forms 78%–79% of the days during the summer. The SCE frequency was determined after analyzing two years of data with empirical orthogonal functions (EOFs) from a limited observational network and satellite imagery. An explanation of the formation mechanism of the SCE will be provided in Part II of this study.

1. Introduction

Atmospheric eddies (or vortices) of various sizes and lifetimes have been observed and studied in several areas along the U.S. West Coast during recent decades. The most frequently studied is the Catalina eddy, which occurs sporadically during the summer in the Southern California Bight. With its horizontal size of 100–200 km and its vertical extent of about 1 km, the Catalina eddy belongs to the meso-β scale. Three mechanisms have been proposed to explain its formation. The first (Bosart 1983; Mass and Albright 1989; Thompson et al. 1997; Ueyoshi and Roads 1993; Ulrickson et al. 1995; Davis et al. 2000; Skamarock et al. 2002) postulates that strong northerly or northwesterly flow at low levels, characterized by a high Froude number,[1] passes over the west-to-east-oriented Santa Ynez Mountains to form a mesoscale lee-side trough. Ageostrophic southerly flow then initiates the eddy. By contrast, the second theory is based on a low-Froude-number flow at the lower levels (Wakimoto 1987; Eddington et al. 1992; Clark and Dembek 1991; Ueyoshi and Roads 1993; Ulrickson et al. 1995). The vorticity necessary to start the eddy is formed by the acceleration of the surface northwesterly flow around the topography rather than over it. The third theory (Dorman 1985; Clark 1994) relates the eddy formation to a Kelvin wave, identifiable as an upward bulge in the marine layer inversion height (with accompanying high surface pressure) that moves northward (often from Baja California, Mexico) at a speed of about 5–8 m s^{-1}. It is postulated that the Catalina eddy forms because the wave cannot progress past the sharp bend in the coast at Point Conception, where it encounters the mean northerly wind. Although they differ substantially from each other, the theories have one common characteristic; that is, the sea level pressure gradient is reversed. They all require lower pressure to the north of the California Bight in order for the eddy to be initiated.

Vortices have been found in several other areas along the west coast of North America. The Midchannel and Gaviota eddies form near the Catalina eddy in the Southern California Bight. Several researchers (Wilczak et al. 1991; Kessler and Douglas 1991; Dorman and Winant 2000) have suggested that the Mid-

[1] The Froude number is defined as

$$\mathrm{Fr} = \frac{U}{\sqrt{g'h}}, \tag{1.1}$$

where U is the upstream wind speed, g' the reduced gravity $g \times \Delta\theta/\theta$ (where $\Delta\theta$ is the difference in potential temperature θ between the bottom and top of the layer), and h the height of the marine boundary layer. The Froude number is often used to determine the flow criticality. If Fr is greater than one, the flow is supercritical, whereas values less than one indicate subcritical flow.

Corresponding author address: Cristina L. Archer, Department of Civil and Environmental Engineering, Stanford University, Stanford, CA 94305.
E-mail: lozej@stanford.edu

channel eddy is formed by the convergence of strong synoptic northwesterly flow and weak easterly flow from the mountains, the latter caused by a local area of low pressure associated with diurnal heating. It forms frequently in the autumn (Wilczak et al. 1991). Dorman (1985) argues that, farther north, the Point Arena and Cape Mendocino eddies are caused by a northward propagating Kelvin wave. Mass and Albright (1989) state that the Vancouver Island eddy is caused by the deflection of a southerly surge formed in response to a pressure drop over Vancouver Island.

Other coastal locations around the world have also been the sites of occasional eddy formation. The South Island eddy in New Zealand (Laing and Reid 1999), where the pressure dip was a consequence rather than a cause of the cyclonic rotation, was perhaps associated with barrier and gap effects from the Southern Alps. The Gulf of Antalya eddy in the Mediterranean Sea (Alpert et al. 1999) originated by convergence, and resulting cyclonic rotation of downslope winds formed on about 20% of the summer days. Convergence of two sea breezes formed a mesoscale eddy at Port Phillip Bay in Australia (Abbs 1986).

Mechanisms such as ageostrophic flow toward an area of low pressure and convergence (either orographically or thermally induced) also occur over land, so it is not surprising that eddies have been identified at inland locations as well. Examples include the Denver Cyclone (Wilczak and Glendening 1988; Wilczak and Christian 1990; Crook et al. 1990, 1991), the Fresno eddy (Seaman and Stauffer 1994), and the Sacramento eddy (Lin and Jao 1995).

The Santa Cruz eddy (SCE), which is the subject of this paper, forms over Monterey Bay, a 20 km $\times$ 40 km bay located $\sim$100 km south of San Francisco Bay. The eddy horizontal size varies from 10 to 40 km, and its lifetime is on the order of hours. The SCE is a shallow circulation, forming within the marine layer, below an inversion. It is smaller than all other North American eddies, except for the Gaviota eddy, which is comparable in size but was recently reclassified as a narrow zone of strong horizontal wind shear, rather than a vortex, by Dorman and Winant (2000). Wilczak et al. (1994), while examining radar observations of surface oceanic currents in Monterey Bay, noted a small cyclonic gyre in the waters of the bay. From this, they postulated that the currents in the water might be driven by winds over the bay. They were able to simulate such an eddy with characteristics similar to the SCE using a numerical model.

In summary, mesoscale eddies are common in the atmosphere. However, most eddies form sporadically, when certain unusual weather conditions occur. The Santa Cruz eddy is an exception in that it forms almost every evening in the summer, as shown later in section 3. Furthermore, it is smaller (in size and lifetime) than all other eddies identified to date.

This study of the SCE is first approached from an observational point of view in Part I of this study (the present paper), where details of the eddy are inferred from a 2-yr database of meteorological observations. Statistical analyses based on empirical orthogonal functions are performed to derive the SCE frequency. Because of the partial picture offered by the relatively sparse network of observations, a numerical approach is then presented in the second part of this paper (Archer and Jacobson 2005, hereafter Part II), in which a theory for the SCE formation is presented within the framework of inviscid flow past a topographic obstacle.

2. SCE observations

a. Satellite imagery

Visible satellite images (Fig. 1) can be used to identify the SCE presence and delineate some of its features. Under typical summer conditions, stratus clouds (i.e., fog) cover most of the eastern Pacific and provide a marker for the rotation associated with the SCE. It typically begins as a tongue of fog that starts to rotate counterclockwise from the southeastern part of Monterey Bay (Figs. 1a,c). Although the main flow off the California coast is northwesterly, the eddy causes surface winds to blow from the east in the northern part of Monterey Bay and advects fog into the otherwise clear Santa Cruz area (see Fig. 2 for the location of Santa Cruz).

The horizontal size of the SCE can vary. It can cover most of Monterey Bay (Figs. 1b,d) or can be limited to the northern or northeastern part of Monterey Bay (Figs. 1a,c). Like the Denver Cyclone and the Catalina eddy, the SCE often has a warm core; that is, it has a warm and dry "eye" in its center (Figs. 1b,d). The SCE can start as early as 1600 Pacific daylight time (PDT)[2] (Fig. 1a), but a fully closed circulation usually does not form until later. For this reason, the SCE can be considered a nighttime phenomenon. Satellite images taken in the early morning after an SCE event sometimes still show the presence of the vortex (e.g., Figs. 1b,d). The eddy never survives past $\sim$1000 PDT, since the strong westerly flow associated with the sea breeze destroys the weaker circulation of the SCE.

b. Surface winds

Data were acquired from 10 surface stations during the summers of 2000 and 2001 from the National Weather Service (through the Unidata datafeed) and the Naval Postgraduate School (NPS) of Monterey [through the real-time environmental information network and analysis system (REINAS) database]. Of the 10 surface stations, 3 were buoys (Fig. 2). Data from

[2] In the rest of this study, the PDT is used, corresponding to -7 h from the coordinated universal time (UTC) in the summer.

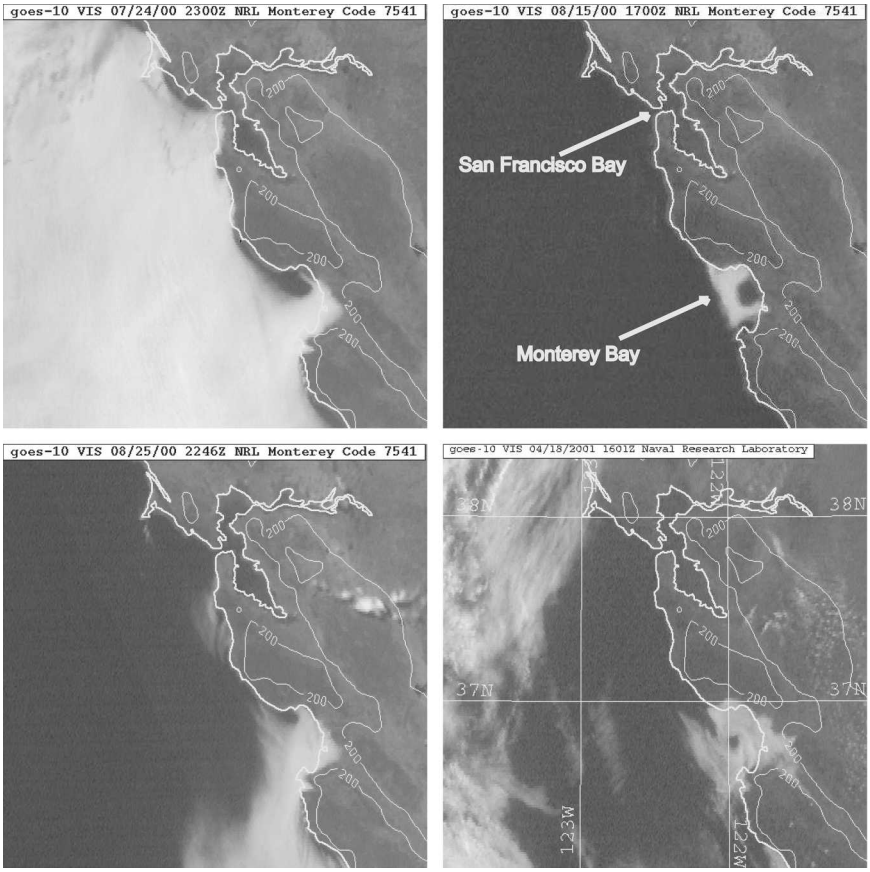

FIG. 1. *Geostationary Operational Environmental Satellite-10* (*GOES-10*) visible satellite images (1-km resolution) of San Francisco Bay and Monterey Bay, showing several examples of cyclonically rotating stratus clouds associated with Santa Cruz eddies: (a) 2300 UTC (1600 PDT) 24 Jul 2000; (b) 1700 UTC (1000 PDT) 15 Aug 2000; (c) 2246 UTC (1546 PDT) 25 Aug 2000; and (d) 1600 UTC (0900 PDT) 18 Apr 2001.

one profiler (Fort Ord) were also provided by the NPS. To determine the relationship between the winds at these stations and the SCE development, special emphasis was placed on the 25 August 2000 event, when the eddy formation and partial evolution could be observed in the satellite imagery. More details can be found in Archer (2004).

The winds observed during the SCE event of 25 August 2000 are shown in Fig. 3. The sea breeze was established in the afternoon, at about 1300 PDT, with westerly winds at Santa Cruz [Long Marine Laboratory (LML)] and Fort Ord (ORD), northwesterly at Monterey (MRY) and buoy M1B, and north-northwesterly at buoys M2B and M4B. Note that the sea breeze was characterized by southwesterly winds at the Watsonville station (WVI). As shown in the satellite image in Fig. 1c, an SCE event started out that afternoon as a small eddy initially limited to the northern part of the bay. The image shows fog being advected toward the Santa Cruz area from the east at about 1600 PDT, but the circulation does not yet appear to be closed at that hour. An hour later, a sudden wind shift from westerly to easterly occurred at LML (not shown). This shift coincided with the beginning of the SCE, since winds at all 10 locations were for the first time consistent with a closed circulation. At WVI, the transition from sea breeze to SCE was more gradual, as winds slowly turned from southwesterly at 1300 PDT to southerly at 1700 PDT (not shown).

Later, this SCE developed into a larger eddy, as shown in Fig. 3b. In fact, by 2000 PDT most of the stations indicated the presence of a larger SCE over the bay. Winds had shifted to southwesterly at MRY and ORD, southeasterly at WVI, and northwesterly at M1B. The two buoys outside of the Monterey Bay—that is, M2B and M4B—showed the undisturbed north-northwesterly main flow, and the Salinas (SNS) site had a strong flow into the Salinas Valley. The eddy dissipated by 2200 PDT and was replaced by light and variable winds, as shown in Fig. 3c.

Five hours after the eddy dissipated, at approximately 0300 PDT, a second circulation formed, similar

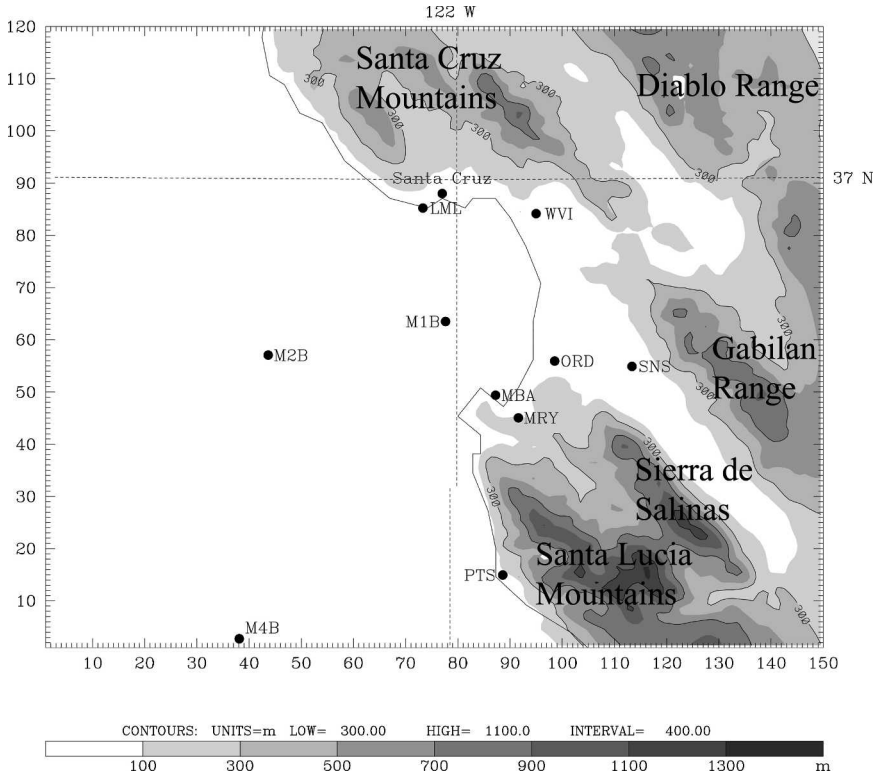

FIG. 2. Topography details of the Monterey Bay area (m; shaded) and station locations. The area shown coincides with the high-resolution domain (domain 2) used for the numerical simulations described in Part II of this study.

in size to the previous one, but characterized by generally lower wind speeds (Fig. 3d). It lasted until about 0800 PDT. The formation of a second circulation was not unique to the 25 August 2000 case. In fact, two consecutive eddies were a commonly observed feature in the database, with some cases even showing three vortices in one night. In no case was one single eddy able to last the entire night. Hereafter, the eddy forming in the evening is indicated as either the "first" or the "evening" eddy, while the eddy forming at night is called either the "second" or the "nocturnal" eddy.

c. Sea level pressure and temperature

Surface wind analysis was necessary to identify the main characteristics and timings of the SCE, but it could not provide much insight into the eddy formation mechanism. As noted earlier, past studies have consistently found surface pressure patterns to be important factors in the eddy formation. Sea level pressures were thus analyzed for two key locations (MRY and LML) for 24 h beginning at 1200 PDT on 25 August (Fig. 4a). Sea level pressure decreased toward the north of the Monterey Bay, as the most northern location (LML) had an average sea level pressure 0.2–0.4 hPa lower than the southernmost location (MRY). This south-to-north pressure gradient[3] suggests the presence of a local low on the southern side of the Santa Cruz Mountains, near Santa Cruz.

The pressure difference (proportional to the pressure gradient strength) between MRY and LML increases before the eddy forms (Fig. 4a); the maximum difference occurred at 1700 PDT on 25 August, just as the eddy reached LML and caused the wind shift from westerly to easterly. The pressure gradient fell after the eddy started, creating a pattern of rising and then falling pressure, which is referred to here as a "pressure bump."[4] Figure 4a shows that the pressure gradient rose again at about 2300 PDT, approximately the same

[3] The standard meteorological convention that the pressure gradient points to lower pressure values (Hucshke 1959) is assumed in this paper. A south-to-north pressure gradient therefore points to the north, where pressures are lower.

[4] The most likely explanation for these pressure bumps is the balance between mass accumulation due to convergence and mass depletion due to rising motion. During either eddy, wind convergence to the center of the eddy causes pressure to rise (and the pressure gradient to fall), since vertical motion is not enough to compensate for the mass accumulation (Holton 1992). In the dissipating stages, mass depletion due to rising motion may become stronger than mass accumulation due to convergence, and the pressure in the center of the eddy may therefore fall again (and thus the pressure gradient may be restored).

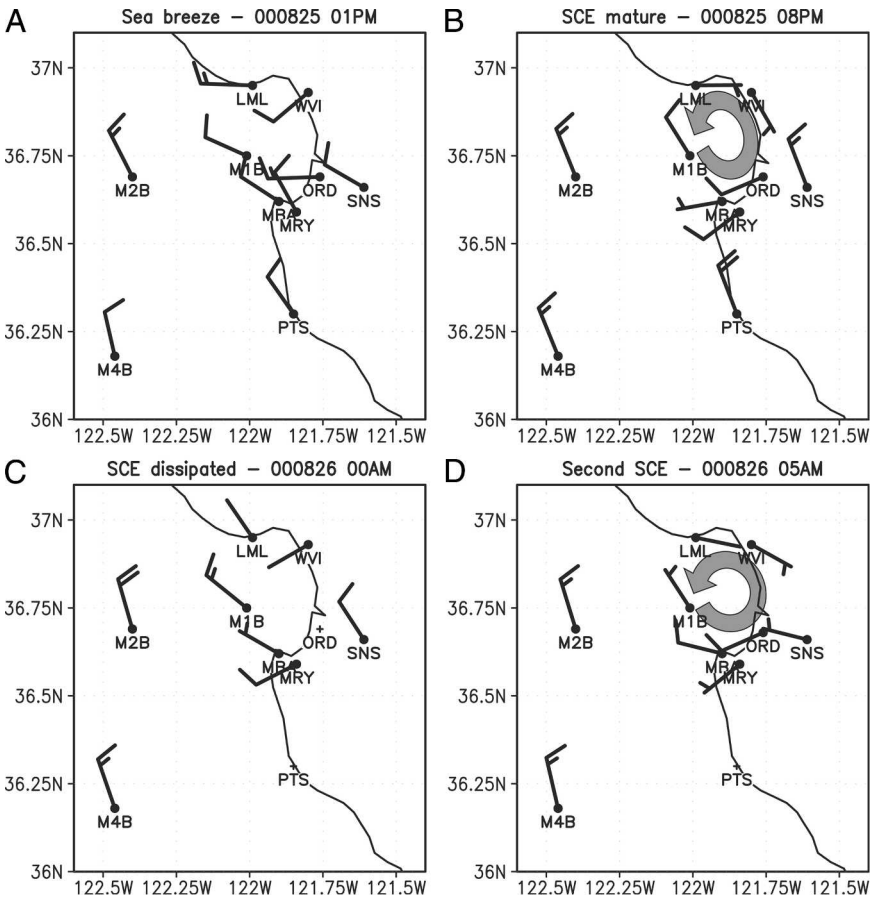

FIG. 3. Observed wind barbs (kt) at key times of the SCE evolution (25 Aug 2000): (a) before the eddy formation, while the sea breeze dominates over Monterey Bay; (b) the (first) mature eddy, occupying the whole bay; (c) the dissipating stage of the (first) SCE, when light and variable winds replace the eddy; and (d) the second SCE in its mature stage.

time as surface winds in Fig. 3c showed the eddy to be dissipated. After a few hours, the pressure gradient decreased again (second pressure bump), at about the same time (~0400 PDT) that surface winds at LML were again consistent with the presence of an SCE in Fig. 3d.

So far, the wind and pressure analysis on 25 August 2000 suggests a strong similarity between the SCE and the Catalina eddy, in that a reversed pressure gradient appears to be the cause of both eddies. However, an extensive analysis of over 100 other days proved this hypothesis to be wrong. In fact, the north-to-south pressure gradient is observed over Monterey Bay during all analyzed days, with and without SCE, and therefore it does not appear to be a sufficient condition for eddy formation. Although, in general, the strength of the south-to-north pressure gradient showed a correlation with the eddy, as seen in Fig. 4 for 25 August 2000, about one-third of the eddy cases exhibited no pressure bumps, perhaps due to comparable amounts of surface convergence and vertical divergence. There were also days without eddies that had a pressure bump. For this reason, the mechanism of the SCE formation cannot be explained solely on the basis of the pressure pattern, which was the fundamental mechanism for most other mesoscale eddies.

If not the SCE, what causes this north-to-south pressure gradient? The Santa Cruz Mountains to the north of Monterey Bay protect the Santa Cruz area from the cold marine air. This allows increased surface heating, which results in an average summer temperature that is about 1.5°C higher than in nearby Monterey (Table 1). Increased surface heating may then form the localized area of low pressure in the northeastern part of Monterey Bay, which would contribute to the south-to-north pressure gradient. Furthermore, the mountains of the Santa Lucia Range to the south of the bay block the main northwesterly flow and may increase the cool marine layer depth in the southern part of the bay (because of both horizontal convergence and suppression of vertical motion by the marine inversion), causing a local area of higher pressure in the Monterey area, a feature consistent with the observations. Thus, the south-to-north gradient seems to be the product of two

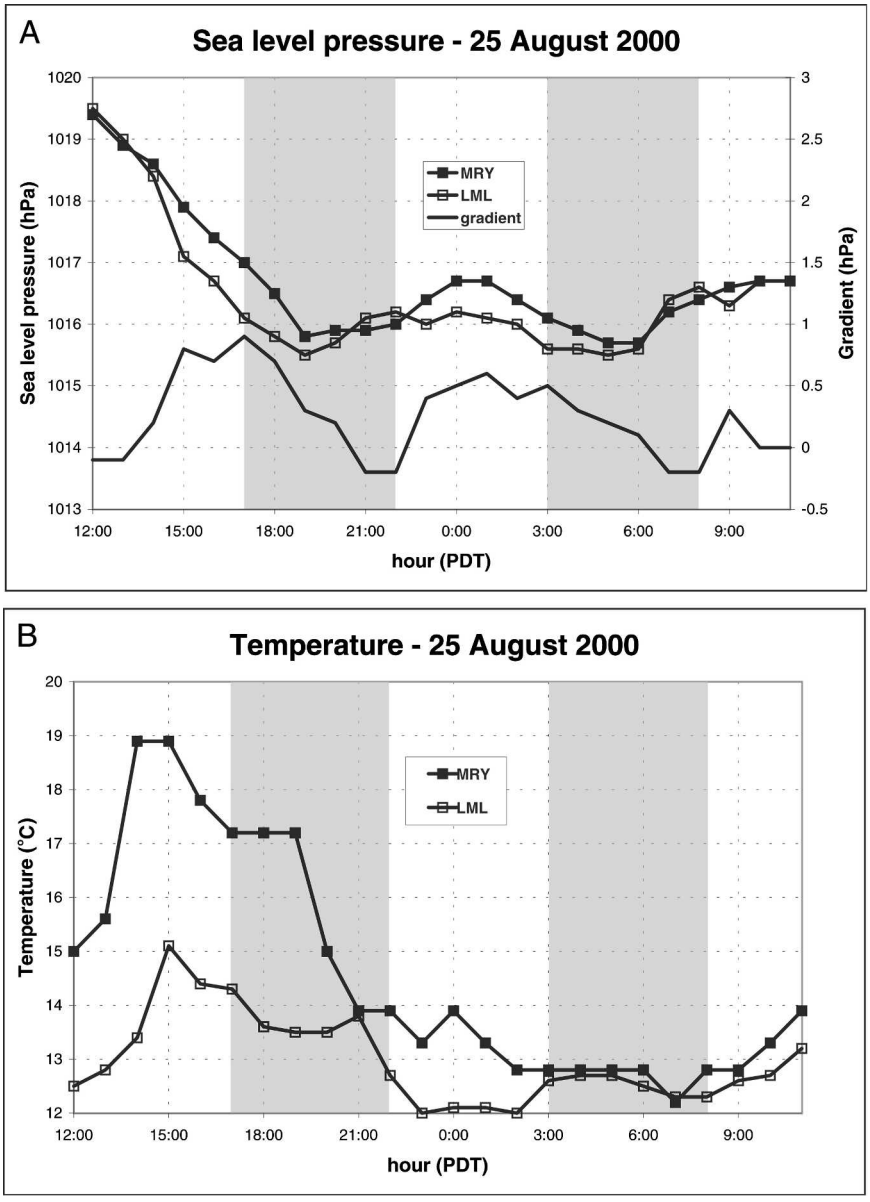

FIG. 4. Time series of (a) sea level pressure and (b) temperature for LML and MRY stations on 25 Aug 2000. The beginning through the end of each eddy is marked by a shaded area.

topographical effects on the steady northwesterly summer winds.

For consistency, higher temperatures are expected in the Santa Cruz area, where sea level pressure was lower (Fig. 4b). However, the diurnal temperature cycle at LML was more typical of a marine location than one would expect for the sheltered Santa Cruz area. Climatology data show that the average monthly temperature in Santa Cruz[5] is 0.4°–1.8°C higher than in Watsonville or Monterey in the summer (Table 1). This apparent inconsistency can be explained by the fact that the LML

TABLE 1. Mean monthly temperature (°C) for the years 1961–90 at some locations along Monterey Bay.

City	May	Jun	Jul	Aug	Sep
Santa Cruz	14.7	16.4	17.3	17.5	17.5
Watsonville	14.3	15.7	16.4	16.7	16.9
Monterey	13.5	14.7	15.5	16.1	16.9

[5] These climatological data come from station 047916, located between downtown Santa Cruz and Capitola, the next city to the east. This station reports temperature and precipitation observations once a day.

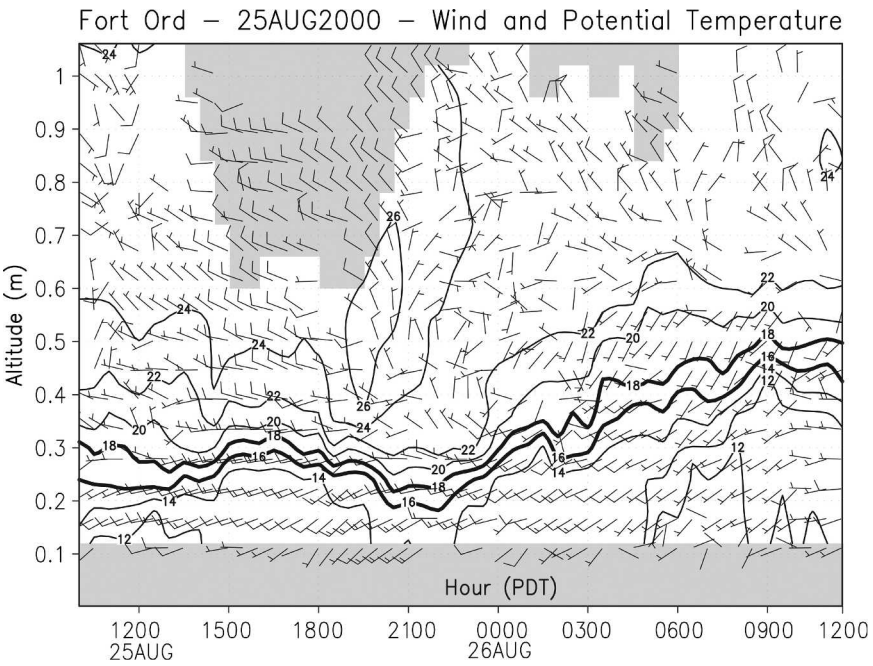

FIG. 5. Fort Ord profiler data for 25 Aug 2000, showing 24 h of wind barbs and virtual temperature (°C) from ground level to 1-km elevation.

station is located about 5 km to the west of the city of Santa Cruz, on the edge of a cliff, exposed to the strong and cool marine flow entering Monterey Bay.

Since temperature generally decreased at LML during the SCE and rose after it dissipated, advection of cool, moist air from the southern bay into the Santa Cruz area may appear to be associated with the presence of an SCE. However, temperature (and relative humidity; not shown) over Monterey Bay is rather uniform at night (Fig. 4b), and therefore no significant cool (and moist) air advection could be associated with the second eddy. From the several cases analyzed, the timing of temperature change is not always synchronized with the SCE. Thus, temperature changes are not a cause of the SCE. This finding will be supported in Part II, where simulations obtained without any heat exchange still show the formation of an SCE.

d. Vertical structure

In addition to the 10 surface observations, a vertical profiler was operating at Fort Ord during both summers under study, retrieving virtual temperature and wind speed and direction every 30 min. These data were useful for evaluating some aspects of the eddy and the marine boundary layer (MBL) evolution. However, given the shallow nature of the SCE, in most cases no additional information could be extracted from the profiler data. Furthermore, observations retrieved at the lowest points (112 and 168 m above ground), which would have been most useful for discerning SCE details, were often incorrect or missing.

For example, the flow at the lowest levels on 25 August 2000 was westerly during the afternoon (Fig. 5). At approximately 1800 PDT, a more southerly component, with higher wind speed around 2000 PDT, was observed for approximately 4 h at the lowest points, followed by lowering and warming of the MBL. The top of the MBL is marked approximately by the 16°–18°C contour lines. This happened at the same time that the SCE was detected at the surface. Light southwesterly winds continued through the night within the layer (and up to the inversion top), together with a rise of the MBL, until the westerly flow associated with the onset of the sea breeze started at about 1100 PDT.

Low-level winds with a southerly component, lowering and then rising of the marine layer ("MBL dip"), and warming near the surface were observed (not always simultaneously) during ~65% of the satellite-confirmed eddy cases. However, in the remaining 35% of these cases, an eddy was present even though none of these indicators was detected from the profiler data. The profiler data showed no evidence of converging (or downslope) flow from either the Gabilan Range or the Sierra de Salinas. This is not surprising, since the tops of the mountains surrounding Monterey Bay are located within or above the inversion. Figure 5 shows temperatures greater than 25°C at elevations of about 1000 m, and hence no cold drainage would be expected.

Profiler data generally showed that the SCE was more likely to occur when the MBL was <500 m deep. When the marine layer is >500 m deep, strong synoptic northwesterlies can pass directly over the Santa Cruz

Mountains and suppress the easterly flow associated with the SCE.

In sum, observations show that SCE events are somewhat correlated with sea level pressure patterns (pressure bumps) and MBL behavior (MBL dips). Since none of these conditions is consistently present prior to eddy formation, another factor must be responsible for the eddy formation. Differential heating, invoked for example for the Midchannel and the Gaviota eddies, is not likely the reason, since the nocturnal SCE forms in the middle of the night, when no strong difference between air temperature above water and land can be detected. Convergence of drainage flow or downslope flow, associated for example with the Gulf of Antalya eddy, does not occur either, because the surrounding mountains are typically warmer than the coastal locations. Bay configuration and topography thus appear to be the only factors that may generate enough curvature and shear in the flow to produce the vorticity necessary for the SCE. However, their effect on the SCE cannot be verified directly from observations. A numerical approach, described in Part II of this study, will explore all the factors contributing to the SCE formation. Below, the observational approach is utilized one more time to determine the climatological importance of the SCE for the Monterey Bay area.

3. SCE statistics

To evaluate how often the SCE forms, one first needs to identify whether or not an eddy formed on a given day. Unfortunately, satellite observations are often not enough. The stratus clouds, whose patterns mark the eddy, often do not penetrate over the sheltered bay; on clear days, no rotation can be detected from the satellite images, and the nocturnal nature of the SCE precludes the use of visible wavelength imagery at night. It is therefore important to make maximum use of those cases when satellite imagery is available to find the observed meteorological behavior that is consistent with the presence (or absence) of SCEs. Once criteria for eddy detection have been devised from cases identified by satellite images, they can be applied to cases without satellite information to establish a final frequency of the SCE.

The database for the statistical analysis consisted of two 31-day periods in July–August 2000 and 2001, during which 18 days were also covered by satellite information. To distinguish eddy days from noneddy days, it would be theoretically possible to analyze *u*- and *v*-wind components at all stations for all hours of each day. However, this approach would not only be tedious and lack objectivity, but it would miss eddy cases that show only at a few stations. What is needed is a method that considers only a few variables, but selected so that they contain most of the information. These advantages are provided by the empirical orthogonal functions (EOFs).

a. Empirical orthogonal functions

Almost 50 yr ago, Lorenz (1956) introduced EOFs as a method of reducing the number of variables required to describe distribution of atmospheric pressure and temperature with minimal loss of information. Since then, the EOF approach has been widely used, and it often goes by various names, such as principal component analysis, factor analysis, and eigenvector analysis. EOF analysis has many desirable properties, such as the fact that the resulting features are based on the characteristics of the data themselves; they are linearly independent of one another; and a measure of their relative importance is provided. This technique also has the advantage of often revealing physically important connections in the data.

Most EOF applications in meteorology have focused on scalar features. For example, Lumley (1981) used EOF analysis to extract coherent structures from turbulent flows. Hardy (1977) suggested a similar approach for classifying wind datasets, an application closely related to this study. Ludwig and Byrd (1980) also applied the concept to vector fields, identifying patterns of variability in the inputs used for a linear diagnostic wind model in order to simplify the resulting calculations. Sirovich (1988) described the analysis of turbulent flows by a similar procedure, and Mahrt (1991) and coworkers (Manning and Frank 1988) applied closely related methods to the analysis of wind variability along an aircraft line of flight. Similarly, Kaihatu et al. (1998) applied EOFs to oceanic surface currents. Ludwig and Street (1995) described a method by which preferred small-scale patterns within a larger scale flow could be determined using EOFs. Dorman and Winant (2000) found the signatures of synoptic and diurnal variations in the EOF analysis of winds in the Santa Barbara Channel.

b. Theory of EOFs

The following description of EOFs is based on Lorenz (1956). Details can be found in Archer (2004). Given a meteorological variable (such as pressure, or the *u* and *v* components of the horizontal wind) observed at a station m ($m = 1 \ldots M$) at time n ($n = 1 \ldots N$), let $\mathbf{P}$ be the $N \times M$ matrix containing the deviations of such variable around its mean ($p_{n,m}$).

The starting point is to find two matrices $\mathbf{Y}$ and $\mathbf{Q}$ such that

$$\mathbf{P} = \mathbf{QY}, \tag{3.1}$$

where $\mathbf{Q}$ and $\mathbf{Y}$ are $N \times M$ and $M \times M$ matrices, respectively. The coefficients $q_{n,k}$ and the vectors $\mathbf{y}_k$ are chosen to minimize the sum of the mean square errors between the observed values $p_{n,m}$ and their approximations given by the linear combination of $q_{n,m}$ and $y_{m,m}$. Note that the vectors $\mathbf{y}_k$ are not a function of time.

A solution to this problem can be obtained by re-

quiring that the matrices **Q** and **Y** are orthonormal and orthogonal, as follows:

$$\mathbf{Y}\mathbf{Y}^{\mathrm{T}} = \mathbf{I}, \tag{3.2a}$$

$$\mathbf{Q}^{\mathrm{T}}\mathbf{Q} = \mathbf{\Lambda}, \tag{3.2b}$$

where **I** is the $M \times M$ unit matrix and $\mathbf{\Lambda}$ is an $M \times M$ diagonal matrix whose diagonal elements are arranged in decreasing order. The superscript T denotes the transpose. By substituting $\mathbf{Q} = \mathbf{P}\mathbf{Y}^{\mathrm{T}}$ [derived from Eq. (3.1)] in (3.2b), one obtains

$$\mathbf{Q}^{\mathrm{T}}\mathbf{Q} = (\mathbf{Y}\mathbf{P}^{\mathrm{T}})(\mathbf{P}\mathbf{Y}^{\mathrm{T}}) = \mathbf{Y}(\mathbf{P}^{\mathrm{T}}\mathbf{P})\mathbf{Y}^{\mathrm{T}} = \mathbf{Y}\,\mathbf{A}\mathbf{Y}^{\mathbf{T}} = \mathbf{\Lambda}, \tag{3.3}$$

which means that the elements of the diagonal matrix $\mathbf{\Lambda}$ are the eigenvalues of $\mathbf{A} = \mathbf{P}^{\mathrm{T}}\,\mathbf{P} = \mathbf{P}\,\mathbf{P}^{\mathrm{T}}$. By design, matrix **A** contains the variances of the meteorological variable of interest. Note that **A** is symmetric by definition. The rows of Y ($\mathbf{y}_{\mathrm{k}}$) are the eigenvectors of **A** and are referred to as EOFs. The columns of Q are referred to as EOF coefficients.

In Eq. (3.2b), the eigenvalues $\lambda_{k,k}$ represent the variances associated with each eigenvector $\mathbf{y}_{\mathrm{k}}$. Since the columns of $^{\mathbf{1}}$ are arranged in decreasing order, the maximum amount of variance is associated with the first eigenvector, and progressively lower variances are associated with the next eigenvectors. It is thus possible to retain only a subset **K** of the **M** eigenvectors; the amount of variance explained by the first K largest eigenvectors is in fact proportional to their sum. This variance can be decided a priori.

The vectors $\mathbf{y}_{\mathrm{k}}$ can be thought of as patterns of variability about the mean. If matrix P contains wind vector components, the resulting $\mathbf{y}_{\mathrm{k}}$s can be plotted at the observing sites on a map to display the important patterns of flow variability. Each $q_{n,k}$ coefficient can be thought of as the intensity of the flow pattern defined by its corresponding EOF $\mathbf{y}_{\mathrm{k}}$ at time t_n.

Figure 6 illustrates how accurately EOFs can represent original data. The u' and v' wind components at the four stations with the highest variances are compared with those estimated from the first six EOFs (corresponding to 95% of the variance) for the 25 August 2000 case.

For Monterey Bay winds, at least one EOF should resemble the SCE, since the eddy represents a deviation from the typical summer flow. This suggests two possible ways of using EOF analysis: 1) on a day-by-day basis, or 2) from the complete body of data. In the first approach, the EOFs can be calculated each day to see if any of them are eddy-like. In the second case, one average eddy-shaped EOF is sought and the magnitude of the coefficients of that particular EOF at each hour is used as a measure of how well the winds correspond to an SCE circulation. Both approaches are described below.

c. Day-by-day EOFs

With this approach, different EOFs were obtained for each day. Twenty-four hourly observations of the u and v components of the horizontal wind retrieved from eight stations were inserted into matrix **P** (24×16) for each of the 62 days considered in the database. The value of K was chosen so that more than 95% of the variance would be retained. In general, K was smaller than 8, meaning that at most the first 8 eigenvectors (out of 16) were used. It was found that the three stations with the highest variances were always LML, WVI, and ORD, which (combined) represented approximately 96% of the total variance of the wind field.

Since the SCE represents a variation superimposed on the mean flow, it was reasoned that the SCE-like pattern would be pronounced enough on eddy days that one of the first three EOFs would be likely to resemble the eddy itself. If such an EOF is found, the day can be classified as an eddy day, otherwise the day can be classified as a non-eddy day.

To illustrate this methodology, the eddy event of 25 August 2000 is presented again. The daily mean flow, in Fig. 7a, was typical of summer days: strong onshore flow in the southern bay and near-zero diurnal average along the more sheltered north bay. The highest variance ($\lambda_{1,1} = 42.4\%$) was associated with the flow pattern (EOF1 or $\mathbf{y}_1$) shown in Fig. 7b. The pattern obviously represents the sea/land-breeze component of the diurnal wind cycle, and this thermally driven flow is consistently a major factor in daily wind changes. When EOF1 has a positive coefficient $q_{n,1}$, the average onshore flow will be augmented by the sea breeze. When the coefficient is negative, the flow is weakened or reversed by the land breeze. The second EOF (Fig. 7c) had the cyclonic pattern associated with the SCE: easterly flow at LML and WVI, southwesterly in the south bay, and west-northwesterly at buoy M1B. This pattern explained 26.4% of the variance. The explained variance dropped to 11% for the third EOF, whose disorganized, convergent pattern had no obvious physical meaning.

In cases when the satellite showed no eddy, the average still showed winds to be generally from the northwest (not shown). The first EOF (explaining ~45% of the variance) still reflected the sea-breeze cycle, but neither the second nor third EOF resembled an SCE.

Since each EOF pattern occurs just as frequently as its exact reverse, depending upon the values of the corresponding coefficients $q_{n,k}$, it is also important to look at the temporal evolution of the time-varying $q_{n,k}$ ($k = 1, \ldots, 3$), shown in Fig. 8. Roughly speaking, positive coefficients for EOF1 are found during sea breezes, and negative coefficients during land breezes. Thus, as expected, the EOF1 coefficients became positive just before noon and stayed positive until the late afternoon. The land-breeze effect is indicated by the more negative values around 0300 PDT. Note that since EOFs represent patterns associated with the deviations of u and v from their means, finding a land-breeze signature

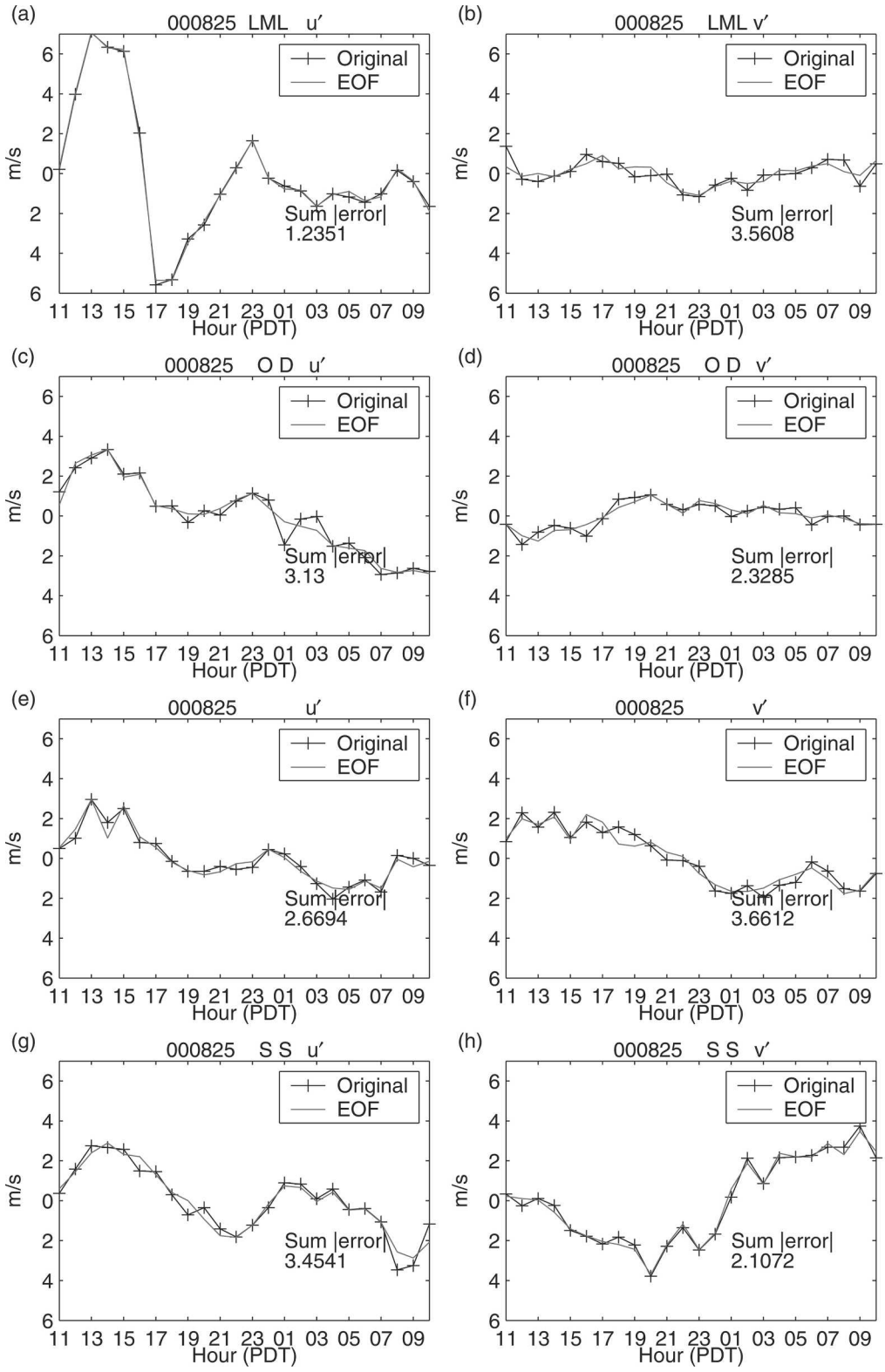

FIG. 6. Trends of u' and v' observed and reconstructed with the first six EOFs, corresponding to 95% of the total variance, for the four stations with highest variances on 25 Aug 2000. The sum of the absolute value of the errors is also shown.

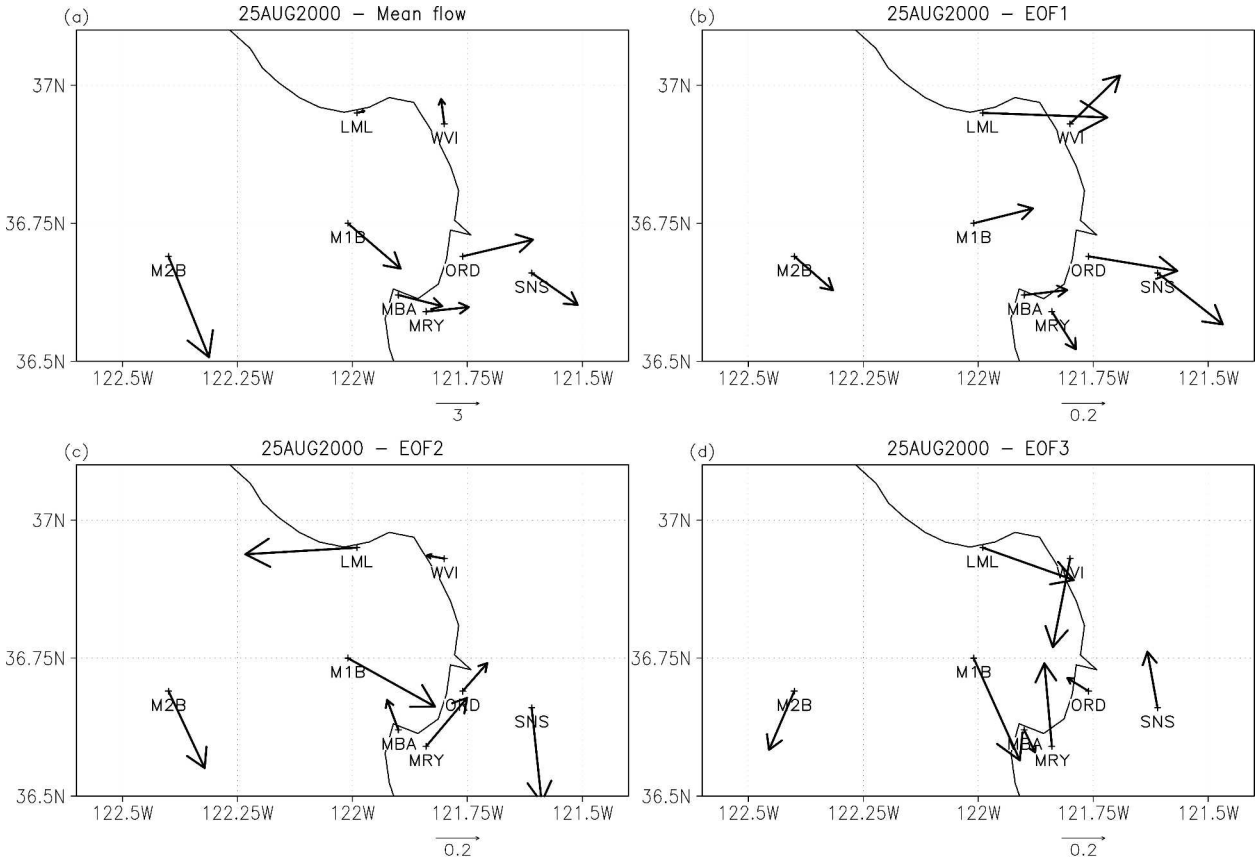

FIG. 7. (a) Mean flow, and (b)–(d) first three EOFs on 25 Aug 2000. Note that the scaling of wind arrows in (a) is different from that in (b)–(d).

in the EOF1 coefficients does not necessarily mean that the actual winds became offshore at night. The effect of the land breeze, although present in the flow, might be masked by the strong synoptic flow.

Similarly, the SCE is associated with EOF2 in Fig. 8. The EOF2 coefficients were negative (indicating a superimposed circulation with negative vorticity) during late afternoon. After that, the coefficients became positive. The highest values indicate that the eddy was strongest around 1900 PDT on 25 August 2000. The reappearance of the eddy is mirrored in the second peak for EOF2 in Fig. 8. The third EOF explained little variance and did not have well-organized patterns. It is not surprising that it had small coefficients and little evidence of diurnal behavior.

These examples indicate that the day-by-day technique can be successful at identifying SCE eddy cases. The results of applying it to each day in the database for which satellite information is available are shown in Table 2, and the final statistics are presented in Table 3. The day-by-day EOF method has a 100% success rate at identifying eddy days (i.e., classifying as "eddy day" a day during which an eddy did occur; outcome indicated as E/E in Table 2). Furthermore, it has a high success rate at identifying noneddy days (63%); that is, classifying as "noneddy day" a day during which no eddy occurred (outcome N/N). The overall success rate (given by the sum of days classified as E/E and N/N in Table 2 over the total number of days) for the day-by-

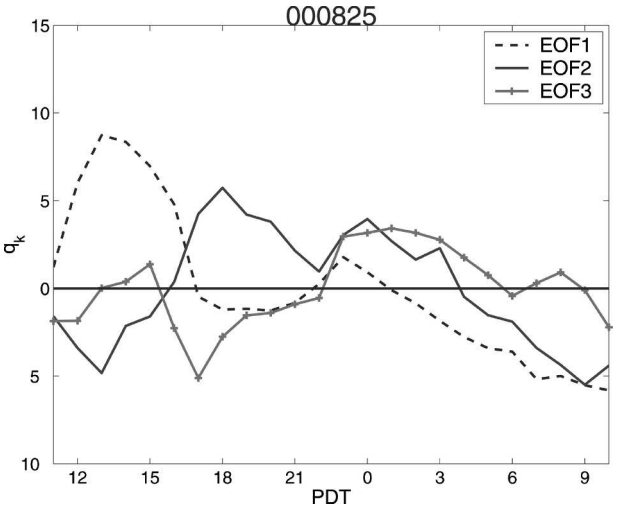

FIG. 8. Trends of $q_{n,k}$ for $k = 1, \ldots, 3$ on 25 Aug 2000.

TABLE 2. Performance of the day-by-day EOF method at identifying eddy (E) or noneddy (N) days. The notation X/Y indicates days classified as X by the EOF method, but identified as Y by the satellite information, where X and Y can either be E or N. Correct outcomes are thus only E/E and N/N.

EOF day-by-day	E/E	E/N	N/E	N/N
No. of days	15	0	3	5
Totals	Eddy: 15 + 0 = 15		No eddy: 3 + 5 = 8	
Percents	15/15 = 100%	0/15 = 0%	3/8 = 37.5%	5/8 = 62.5%
Success rates	Eddy: 100%		No eddy: 62.5%	
	Overall: (15 + 5)/23 = 87%			

day EOF technique was 87% (20/23). The frequency of SCE events obtained by this method is 79% (Table 3).

d. Multiday EOFs

The results discussed to this point suggest that the SCE occurs on a majority of the days in the summer, albeit for only a few hours each day. It seemed worth determining if this was sufficiently frequent that the eddy pattern would explain a major part of the variance in the complete dataset (i.e., the same 62 days used for the day-by-day EOF approach). Therefore, EOFs were determined using all hours available simultaneously from seven[6] of the stations used for the daily EOFs. The resulting EOF patterns are shown in Fig. 9.

The mean and first two EOFs are quite similar to those shown earlier for the 25 August 2000 case. The explained variances are also about the same (42% and 28%, respectively). These results indicate that the coefficients for the second EOF $q_{n,2}$ are a single function that can be used for identifying the eddy days. Figure 10

[6] Stations with variance smaller than that of M2B, including M2B, were excluded because of their small contribution to the total variance.

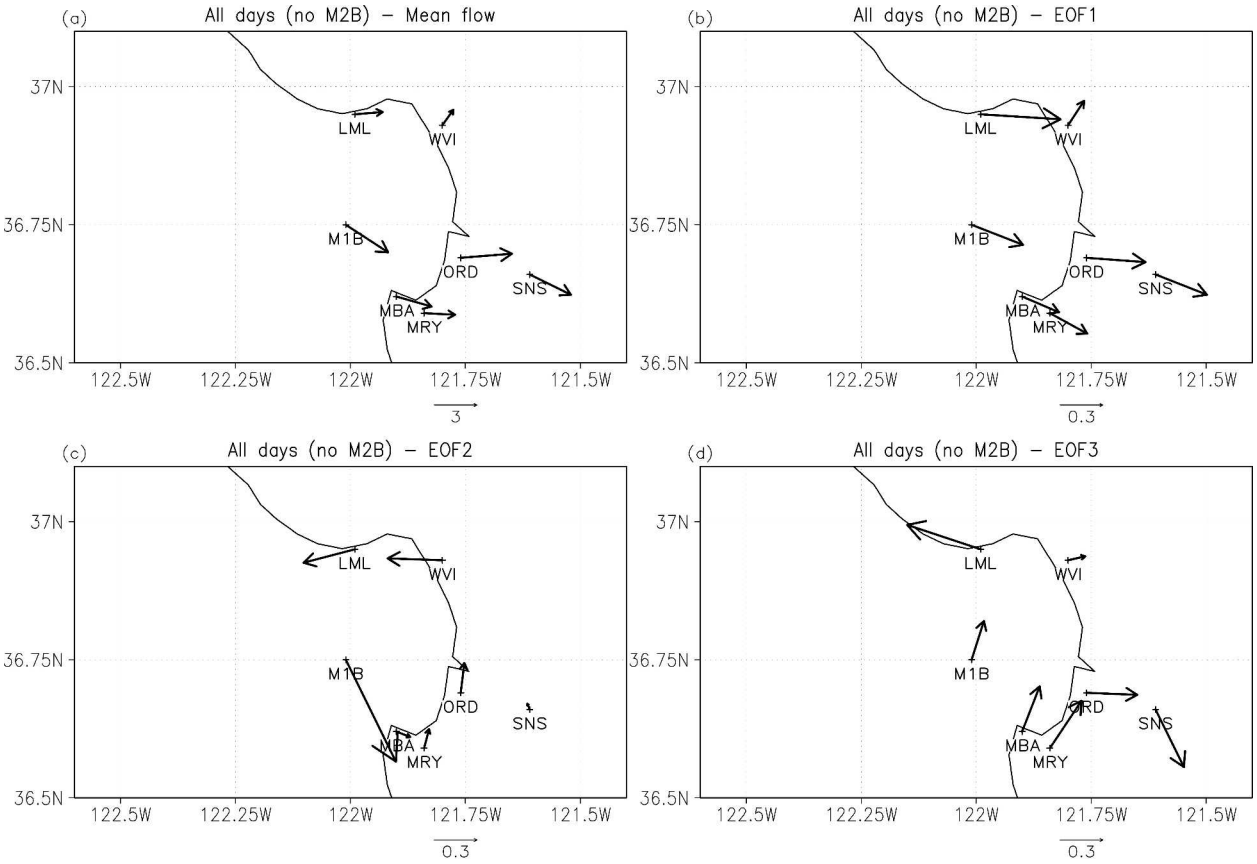

FIG. 9. Same as Fig. 7 but for all days in the database.

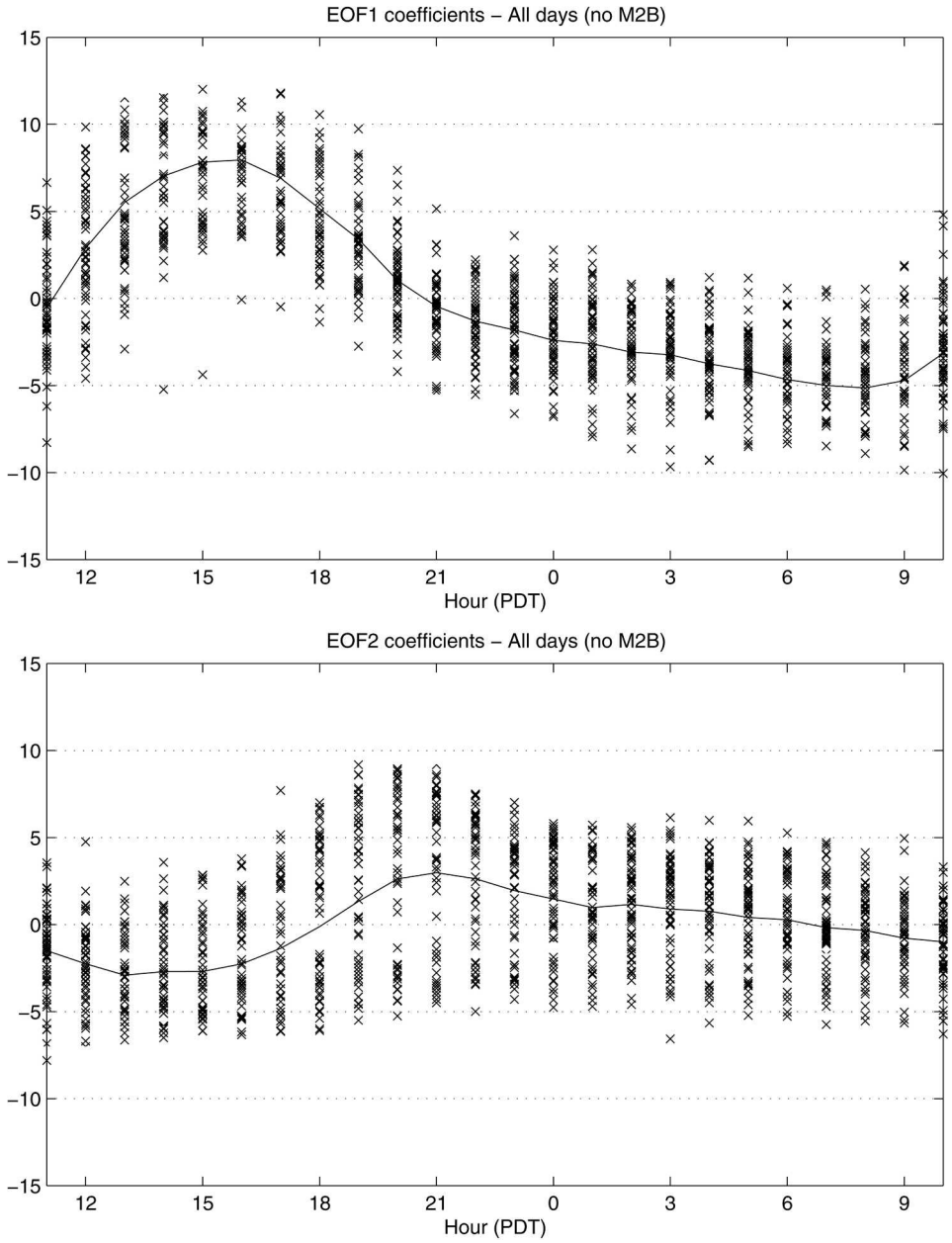

FIG. 10. Values of coefficients $q_{n,1}$ and $q_{n,2}$ for EOF1 and EOF2 obtained from all days in the dataset. The average trend of each coefficient is shown as a solid line.

shows the values of the coefficients for the first two EOFs plotted versus hour of the day for all days combined. Although the scatter from day to day is considerable, the diurnal sea-breeze pattern is clearly visible in Fig. 10a. Figure 10b for EOF2 coefficients shows a clear, but less pronounced diurnal cycle. The hours when eddies generally form (between about 1700 and 2000 PDT) are marked by a bimodal distribution of values; that is, only a few values are found around zero. This gap separates the values into two groups having either positive (eddy pattern) or negative (noneddy pattern) coefficients. This suggests that only two patterns are likely to verify at those hours: either an eddy or no eddy at all. Furthermore, since the mean curve is positive in that time interval, the eddy pattern is more likely to occur.

The days with satellite imagery were used to develop an appropriate threshold, that is, a value such that days with one or more coefficients $q_{n,2}$ above it can be classified as eddy days and vice versa. Several thresholds were tested, varying between 3 (most restrictive) and -1 (most inclusive). No threshold had a 100% success

TABLE 3. Frequency of the SCE estimated from different methods.

	EOF day-by-day		EOF multiday		Satellite	
No. of days	Eddy	No eddy	Eddy	No eddy	Eddy	No eddy
Satellite	18	5	18	5	18	5
Nonsatellite	28	7	27.8	7.2	0	0
Total	46	12	45.8	12.2	18	5
Frequency	46/(46 + 12)	12/(46 + 12)	45.8/(45.8 + 12.2)	12.2/(45.8 + 12.2)	18/(18 + 5)	5/(18 + 5)
	79%	21%	79%	21%	78%	22%

rate at identifying eddy days, a desirable feature that the previous method showed. With the multiday approach, by definition, one single eddylike pattern (EOF2) is used to identify all eddies, no matter what their size, duration, or center might be. It is therefore likely that some eddy days might not match the imposed SCE pattern very well. Similarly, it is possible that some days characterized by strong shear in the Santa Cruz area might be wrongly classified as eddy days. With this limitation in mind, the best threshold appeared to be 3, since it had the highest success rate (93%) at identifying eddy days, as opposed to 86%–89% for thresholds between 2 and −1 (not shown). Although its overall performance is only 78% (Table 4), it was preferred over the 0 and −1 thresholds, which both had 87% overall performances, but lower success rates on eddy days. Based on threshold 3, the frequency of eddy days as determined from the multiday approach was 79% (Table 3).

In summary, the application of the EOF technique to the SCE case was overall successful at identifying eddy and noneddy days, especially with the day-by-day approach. Since the SCE is such a common occurrence over Monterey Bay, it was not surprising that its signature was present in the variance of the wind field. However, results from the EOF analysis should only be interpreted qualitatively and not quantitatively. Trends of $q_{n,k}$ from Fig. 8 simply suggest that conditions compatible with the eddy presence were detected twice that night. The exact hours and duration of these conditions cannot be reliably inferred from this plot. Such limitation would be less significant if the SCE were a stationary feature that formed and stayed in the same place at all times. Since it moves around instead, matching one single eddylike pattern to either all days of the summer (multiday approach) or even just all the hours of a day (day-by-day approach) can be difficult. This study suggests that future applications of the EOF technique will be more succesful at identifying features that are stationary and do not vary considerably in size.

4. Summary and conclusions

This study focused on the observation aspects of the SCE. Surface winds, satellite imagery, and other data from the summers of 2000 and 2001 were used to determine its characteristics, timing, and frequency. To determine eddy frequency, two methods were devised: 1) empirical orthogonal functions (EOFs) derived from daily winds observed at 10 stations, and 2) the magnitude of a single, eddylike EOF derived from all available hours of data. Satellite observations for 18 days provided reliable determinations of eddy occurrence that could be used to test the performance of each method.

Both EOF methods predicted 15 eddy days out of 18 (83%) and missed 17%, but the day-by-day approach had a better overall performance (87% versus 78%). Assuming that error rates for satellite days also applied to other days, it was found that the SCE forms with a frequency of 78%–79% of the days in the middle of the summer. Given its high frequency, the SCE formation cannot be explained by any unusual weather events, but rather by some common conditions for the Monterey Bay area.

Most of the other mesoscale eddies show a localized area of low pressure near the circulation center prior to their formation. In the SCE case too, a south-to-north pressure gradient suggests the presence of a local low pressure area near Santa Cruz. However, this north-to-south pressure gradient is always present over Monterey Bay, regardless of whether an eddy forms or not.

Surface winds consistent with the presence of a closed cyclonic circulation over the Monterey Bay are

TABLE 4. Same as Table 2 but for the multiday EOF method.

EOF multiday	E/E	E/N	N/E	N/N
No. of days	14	1	4	4
Totals	Eddy: 14 + 1 = 15		No eddy: 4 + 4 = 8	
Percents	14/15 = 93%	1/15 = 7%	4/8 = 50%	4/8 = 50%
Success rates	Eddy: 93%		No eddy: 50%	
	Overall: (14 + 4)/23 = 78%			

often found more than once per night, suggesting that two different eddy instances form at different times. Sea level pressure analysis confirmed this finding. A first vortex (evening eddy) forms in the late afternoon and dissipates after a few hours. After that, a second vortex (nocturnal eddy) might form in the early morning and is destroyed before the sea breeze starts. The strength of the south-to-north pressure gradient, as measured by the pressure difference between Monterey and Santa Cruz, has hourly variations that generally correlate well with the SCE timings, as it generally reaches its maximum before either eddy starts and it either drops or stays constant while the eddy develops. These trends of rising and falling pressure ("pressure bumps") are perhaps due to greater convergence at the surface than divergence aloft. Pressure bumps were observed during 66% of the SCE cases. However, pressure bumps were observed also during some noneddy days. It appears therefore that pressure patterns are not the driving mechanism for the SCE formation but rather a consequence of its converging circulation.

Although a denser network of observations would be useful, a statistical analysis of surface winds observed at a limited number of stations appeared sufficient to identify the SCE main characteristics and frequency. However, it could not provide a final answer about the SCE formation mechanism. A modeling approach, described in Part II of this work will allow not only verification of the observational findings about pressure patterns and eddy timings, but also evaluation of the importance of factors such as topography or diurnal cycle by sensitivity analyses.

Acknowledgments. We thank Wendel Nuss [Naval Postgraduate School of Monterey (NPS)] for providing some of the surface data; Dick Lind (NPS) for providing most of the surface data and all the profiler data; and William T. Thompson and Stephen D. Burk (U.S. Naval Research Laboratory of Monterey) for their suggestions. This work was supported by the National Science Foundation (NSF) and by the National Aeronautics and Space Administration (NASA).

REFERENCES

Abbs, D. J., 1986: Sea-breeze interactions along a concave coastline in southern Australia: Observations and numerical modeling study. *Mon. Wea. Rev.,* **114,** 831–848.

Alpert, T., M. Tzidulko, and D. Iziksohn, 1999: A shallow, short-lived meso-β cyclone over the Gulf of Antalya, eastern Mediterranean. *Tellus,* **51A,** 249–262.

Archer, C. L., 2004: The Santa Cruz Eddy and U.S. wind power. Ph.D. thesis, Stanford University, 190 pp.

——, and M. Z. Jacobson, 2005: The Santa Cruz Eddy. Part II: Mechanisms of formation. *Mon. Wea. Rev.,* in press.

Bosart, L. F., 1983: Analysis of a California Catalina event. *Mon. Wea. Rev.,* **111,** 1619–1633.

Clark, J. H., 1994: The role of Kelvin waves in evolution of the Catalina eddy. *Mon. Wea. Rev.,* **122,** 838–850.

——, and S. R. Dembek, 1991: The Catalina eddy event of July 1987: A coastally trapped mesoscale response to synoptic forcing. *Mon. Wea. Rev.,* **119,** 1714–1735.

Crook, N. A., T. L. Clark, and M. W. Moncrieff, 1990: The Denver cyclone. Part I: Generation in low Froude number flow. *J. Atmos. Sci.,* **47,** 2725–2742.

——, ——, and ——, 1991: The Denver cyclone. Part II: Interaction with the convective boundary layer. *J. Atmos. Sci.,* **48,** 2109–2126.

Davis, C., S. Low-Nam, and C. F. Mass, 2000: Dynamics of a Catalina eddy revealed by numerical simulation. *Mon. Wea. Rev.,* **128,** 2885–2904.

Dorman, C. E., 1985: Evidence of Kelvin waves in California's marine layer and related eddy generation. *Mon. Wea. Rev.,* **113,** 827–839.

——, and C. D. Winant, 2000: The structure and variability of the marine atmosphere around the Santa Barbara channel. *Mon. Wea. Rev.,* **128,** 261–282.

Eddington, L. W., J. J. O'Brien, and D. W. Stuart, 1992: Numerical simulation of topographically forced mesoscale variability in a well-mixed marine layer. *Mon. Wea. Rev.,* **120,** 2881–2896.

Hardy, D. M., 1977: Empirical eigenvector analysis of vector observations. *Geophys. Res. Lett.,* **4,** 319–320.

Holton, J. R., 1992: *An Introduction to Dynamic Meteorology.* Academic Press, 511 pp.

Hucshke, R. E., 1959: *Glossary of Meteorology.* Amer. Meteor. Soc., 638 pp.

Kaihatu, J. M., R. A. Handler, G. O. Marmorino, and L. K. Shay, 1998: Empirical orthogonal function analysis of ocean surface currents using complex and real-vector methods. *J. Atmos. Oceanic Technol.,* **15,** 927–941.

Kessler, R. C., and S. G. Douglas, 1991: Numerical simulation of topographically forced mesoscale variability in a well-mixed marine layer. *J. Appl. Meteor.,* **30,** 633–651.

Laing, A. K., and S. J. Reid, 1999: Evidence of mesoscale lows off the west coast of New Zealand. *Wea. Forecasting,* **14,** 369–383.

Lin, Y. L., and I. C. Jao, 1995: A numerical study of flow circulations in the Central Valley of California and formation mechanisms of the Fresno Eddy. *Mon. Wea. Rev.,* **123,** 3227–3239.

Lorenz, E. N., 1956: Empirical orthogonal functions and statistical weather prediction. Science Rep. 1, Statistical Forecasting Project, Dept. of Meteorology, Massachusetts Institute of Technology, 49 pp.

Ludwig, F. L., and G. Byrd, 1980: A very efficient method for deriving mass consistent flow fields from wind observations in rough terrain. *Atmos. Environ.,* **14,** 585–587.

——, and R. L. Street, 1995: Modification of multiresolution feature analysis for application to three-dimensional atmospheric wind fields. *J. Atmos. Sci.,* **52,** 139–157.

Lumley, J. L., 1981: Coherent structures in turbulence. *Transition and Turbulence,* R. E. Meyer, Ed., Academic Press, 215–242.

Mahrt, L., 1991: Eddy asymmetry in the sheared heated boundary layer. *J. Atmos. Sci.,* **48,** 472–492.

Manning, K. W., and H. Frank, 1988: Eigenstructure of eddy microfronts. *Tellus,* **40A,** 107–119.

Mass, C. F., and M. D. Albright, 1989: Origin of the Catalina eddy. *Mon. Wea. Rev.,* **117,** 2405–2436.

Seaman, N. L., and D. R. Stauffer, 1994: The Fresno eddy: Numerical investigation of a mesoscale wind feature of the San Joaquin Valley using the Penn State/NCAR MM5. Preprints, *Sixth Conf. on Mesoscale Processes,* Portland, OR, Amer. Meteor. Soc., 572–575.

Sirovich, L., 1988: Analysis of turbulent flows by means of empirical orthogonal functions. Center for Fluid Mechanics Rep. 90–212, Brown University, Providence, RI, 40 pp.

Skamarock, W. C., R. Rotunno, and J. B. Klemp, 2002: Catalina

eddies and coastally trapped disturbances. *J. Atmos. Sci.,* **59,** 2270–2278.
Thompson, W. T., S. D. Burk, and J. Rosenthal, 1997: An investigation of the Catalina eddy. *Mon. Wea. Rev.,* **125,** 1135–1146.
Ueyoshi, K., and J. O. Roads, 1993: Simulation and prediction of the Catalina eddy. *Mon. Wea. Rev.,* **121,** 2975–3000.
Ulrickson, B. L., J. S. Hoffmaster, J. Robinson, and D. Vimont, 1995: A numerical modeling study of the Catalina eddy. *Mon. Wea. Rev.,* **123,** 1364–1373.
Wakimoto, R. M., 1987: The Catalina eddy and its effects on air pollution over southern California. *Mon. Wea. Rev.,* **115,** 837–855.
Wilczak, J. M., and T. W. Christian, 1990: Case study of an orographically induced, mesoscale vortex (Denver Cyclone). *Mon. Wea. Rev.,* **118,** 837–855.
——, W. F. Dabberdt, and R. A. Kropfli, 1991: Observations and numerical-model simulations of the atmospheric boundary layer in the Santa Barbara coastal region. *J. Appl. Meteor.,* **30,** 652–673.
——, and J. W. Glendening, 1988: Observations and mixed-layer modeling of a terrain-induced mesoscale gyre: The Denver Cyclone. *Mon. Wea. Rev.,* **116,** 1599–1622.
——, W. D. Neff, D. Ruffieux, and J. Schmidt, 1994: Atmospheric and oceanic mesoscale flows in the Monterey Bay, California region. Preprints, *Second Int. Conf. on Air–Sea Interaction and on Meteorology and Oceanography of the Coastal Zone,* Lisbon, Portugal, Amer. Meteor. Soc., 196–197.